# Modelling the Frequency Dependence of the Open-Circuit Voltage of a High-$T_c$ Superconducting Dynamo

Mark D. Ainslie, *Senior Member, IEEE,* Loïc Quéval, Ratu C. Mataira, and Chris W. Bumby

***Abstract*—A high-$T_c$ superconducting (HTS) dynamo enables the injection of large DC currents into a superconducting circuit, without the requirement for current leads. In this work, we attempt to explain the frequency dependence of such dynamos/flux pumps reported in the literature, where it is observed that the rate at which the open-circuit DC voltage increases reduces with increasing frequency, in contrast to the expected linear behaviour. Heat generated in the HTS wire has been the common explanation given to date for this phenomenon. Here we offer an alternative explanation: the interaction between and current flow in the different layers of the HTS wire as the frequency of the dynamo increases. Our claim is based on numerical analysis using a segregated *H*-formulation finite-element model of the HTS dynamo benchmark problem that is extended to include the full HTS wire architecture and coupled with a thermal model. This framework enables us to efficiently model the relative movement between the rotating room-temperature permanent magnet and the stationary HTS wire and to study the impact of the frequency of rotation and temperature on the open-circuit DC voltage of the dynamo.**

***Index Terms*—HTS dynamo, *H*-formulation, HTS modelling, flux pump, finite-element modelling**

## I. Introduction

A high-$T_c$ superconducting (HTS) dynamo [1-3] enables the injection of large DC currents into a superconducting circuit, without the requirement for current leads [4], which can impose a substantial heat load on the cryogenic system. This has significant potential to be used to energise HTS coils in NMR/MRI magnets [5] and superconducting rotating machines [4]. Several different numerical models have now been developed [6] as useful and cost-efficient tools to explain and further examine experimental results, as well as optimise and improve dynamo/flux pump design. It was shown recently in Mataira *et al.* [7, 8] that the open-circuit voltage can be explained well – most importantly, with good quantitative agreement – using classical electromagnetic theory. The DC output voltage obtained from an HTS dynamo arises naturally from a local rectification effect caused by overcritical eddy currents [7-12]: an effect that has been observed in HTS materials as far back as Vysotsky *et al*. [13]. The gap dependence of the open-circuit voltage computed by Ghabeli and Pardo [14] also agrees with experiments. In [14], it is also shown that this voltage is independent of the critical current density, $J_c$, when the superconductor is fully penetrated by supercurrents. Since these overcritical eddy currents must recirculate in the HTS wire, and can co-exist with a transport current, the wire width is a key parameter and [15] shows that this should be sufficiently large so that the eddy and transport currents do not drive the full width of the wire into the flux-flow regime.

In this work, we attempt to explain the frequency dependence of HTS dynamos reported in the literature [16-19], where it is observed that the rate at which the open-circuit DC voltage increases reduces with increasing frequency, in contrast to the expected linear behaviour. The common explanation for this frequency-dependent behaviour is that the heat generated in the HTS wire is the cause [16-19]. An alternative explanation is offered here: the interaction between and current flow in the different layers of the HTS wire as the frequency of the dynamo increases.

To support our hypothesis, we use a segregated ***H***-formulation finite-element model [20] as applied to the HTS dynamo benchmark problem [6]. The results when modelling only the HTS layer of the wire are compared with a model of the full HTS wire architecture that includes the substrate and stabiliser layers. Finally, the electromagnetic model is coupled with a thermal one to examine the effect of the heat generated in the wire.

## II. Modelling Framework

### A. HTS Dynamo Overview

Manuscript receipt and acceptance dates will be inserted here. The work of Mark D. Ainslie was supported by the Engineering and Physical Sciences Research Council (EPSRC) Early Career Fellowship EP/P020313/1. This work was also supported by the Royal Society of New Zealand Marsden Fund grant no. MFP-VUW1806 and EolSupra20 project ANR-10-LABX-0040-LaSIPS. *(Corresponding author: Mark D. Ainslie.)*

M. D. Ainslie is with the Bulk Superconductivity Group, Department of Engineering, University of Cambridge, Trumpington Street, Cambridge CB2 1PZ, United Kingdom (e-mail: mark.ainslie@eng.cam.ac.uk).

L. Quéval is with the Group of Electrical Engineering – Paris (GeePs), University of Paris-Saclay, CentraleSupélec, CNRS, Gif-sur-Yvette 91192, France.

R. C. Mataira and C. W. Bumby are with the Robinson Research Institute, Victoria University of Wellington, Lower Hutt 5046, New Zealand.

Color versions of one or more of the figures in this paper are available online at http://ieeexplore.ieee.org.

Digital Object Identifier will be inserted here upon acceptance.

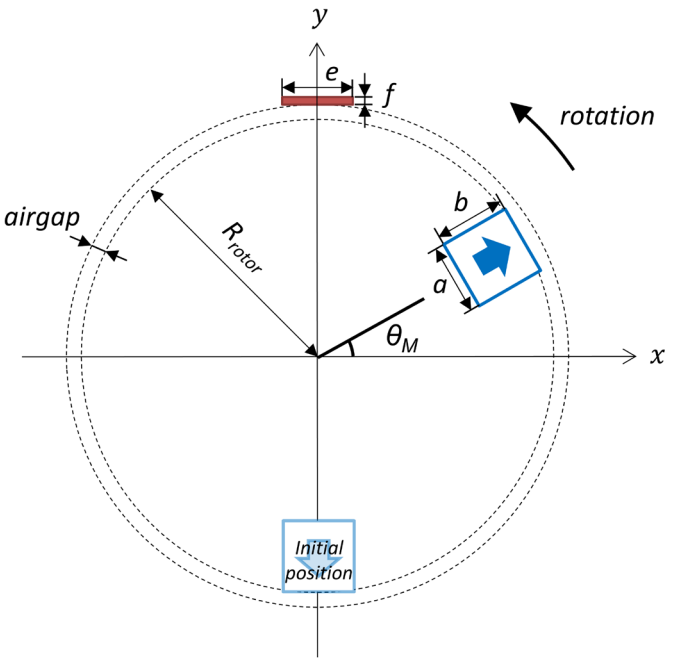


Fig. 1. Geometry of the HTS dynamo model. A permanent magnet rotates anticlockwise past a stationary HTS wire. Reproduced from [6].

The geometry of the HTS dynamo is shown in Fig. 1 with the assumed parameters in Table I, which are based on the 2D HTS dynamo benchmark problem recently proposed in [6] and correspond to the experimental setup in [21].

TABLE I. HTS DYNAMO MODEL ASSUMED PARAMETERS

| | | |
|---|---|---|
| **Permanent magnet (PM)** | ***Width, a*** | 6 mm |
| | ***Height, b*** | 12 mm |
| | ***Active length (depth), L*** | 12.7 mm |
| | ***Remanent flux density, $B_r$*** | 1.25 T |
| **HTS stator wire** | ***Width, e*** | 12 mm |
| | ***Thickness, f*** | 1 μm |
| | ***Critical current, $I_{c0}$ [self-field, 77 K]*** | 283 A |
| | ***n value*** | 20 |
| ***Rotor radius, $R_{rotor}$*** | | 35 mm |
| ***Distance between PM & HTS wire, airgap*** | | 3.7 mm |
| ***Frequency of rotation*** | | 10 – 500 Hz |
| ***Number of cycles*** | | 10+ (see text) |

### *B. Segregated **H**-Formulation Finite-Element Model*

The model implements the 2D ***H***-formulation [22-28], where the independent variables are the components of the magnetic field strength, $\boldsymbol{H} = [H_x, H_y, 0]$, and the governing equations are derived from Ampere's and Faraday's laws. The current density, $\boldsymbol{J} = [0, 0, J_z]$, and electric field, $\boldsymbol{E} = [0, 0, E_z]$, are parallel to each other, such that $\boldsymbol{E} = \rho\boldsymbol{J}$. The nonlinear resistivity, $\rho(J)$, of the superconductor is simulated using an $E$-$J$ power law [29-31]:

$$\boldsymbol{E} = \frac{E_0}{J_c}\left|\frac{\boldsymbol{J}}{J_c}\right|^{n-1}\boldsymbol{J} \tag{1}$$

where $E_0 = 1$ μV/cm is the electric field criterion, $J_c$ is the critical current density of the superconductor and $n$ defines the steepness of the transition between the superconducting state and the normal state [32, 33]. For simplicity, the critical current density of the superconductor, $J_c$, is assumed to be constant and equal to $J_{c0}$ such that $J_{c0} = I_{c0}/(e{\cdot}f) = 2.358 \times 10^{10}$ A/m$^2$. $e$ and $f$ are the width and thickness of the HTS layer of the wire, respectively (see Fig. 1 and Table I).

The induced voltage, or instantaneous output voltage, developed along the superconductor, $V(t)$, is calculated from the electric field, $E_z(t)$, averaged over the cross-section, $E_{ave}$ [6], such that:

$$V(t) = -L\cdot E_{ave}(t) = -L\frac{1}{S}\int_S E_z(t)\cdot dS \tag{2}$$

where $L$ is the active length (depth) of the PM and $S$ is the cross-section of the HTS wire.

Under open-circuit conditions, no net transport current flows, and a constraint in the model is implemented such that, at all times:

$$I(t) = \int_S J_z(t)\cdot dS = 0 \tag{3}$$

Finally, the DC output voltage of the dynamo, $V_{DC}$, is calculated by

$$V_{DC} = \frac{1}{T}\int_t^{t+T} V(t')\,dt' \tag{4}$$

as the average value of the induced voltage over one period of rotation, $T$, in the steady-state.

The segregated model, implemented in COMSOL Multiphysics 5.4, consists of a *magnetostatic* PM model and a *time-dependent* ***H***-formulation HTS wire model. The former is coupled unidirectionally to the latter using electromagnetic boundary conditions and a rotation operator to mimic the movement of the PM [20, 34, 35], as shown in Fig. 2. This avoids the need for modelling moving parts (e.g., using a moving mesh) and significantly reduces the number of mesh elements, resulting in a fast and efficent model [6].

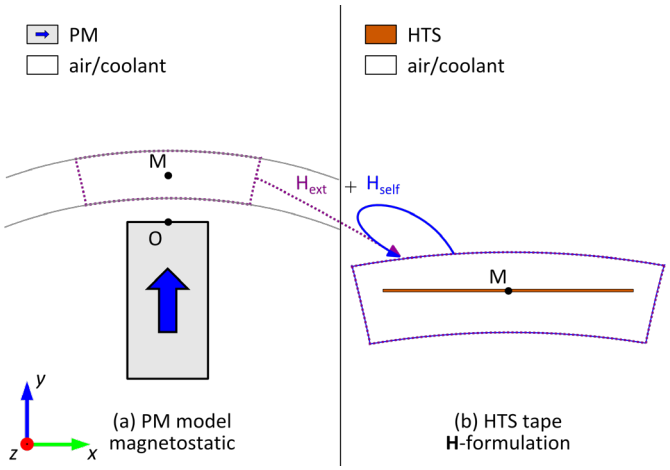


Fig. 2. Segregated finite-element model: (a) *magnetostatic* PM model, (b) *time-dependent* ***H***-formulation HTS wire model. Reproduced from [6].

On the outer boundary of the ***H***-formulation model, the sum of the applied field, $\boldsymbol{H}_{ext}$, and the self-field, $\boldsymbol{H}_{self}$, is applied as a Dirichlet boundary condition. $\boldsymbol{H}_{ext}$ is obtained by rotating the field of a static permanent magnet [6] and $\boldsymbol{H}_{self}$, created by the supercurrent flowing in the HTS wire, is obtained at each time step by numerical integration of the 2D Biot-Savart law over the HTS wire subdomain [20, 35].

### C. Full HTS Wire Architecture Model

The full HTS wire architecture model is based on SuperPower's Surround Copper Stabilizer 2G HTS wire, SCS12050, assuming a 50 µm Hastelloy C-276 substrate and top and bottom 20 µm copper stabilizer layers [36], ignoring any copper surrounding the sides of the wire. A cross-sectional view of the modelled full wire is shown in Fig. 3. The resistivity of the substrate is assumed to be temperature-independent with $\rho_{sub} = 1.25 \times 10^{-6}$ Ωm [36, 37]. The resistivity of the copper is assumed to be temperature-dependent with $\rho_{Cu} = \rho_{Cu0}(1+\alpha(T\text{-}293.15))$, where $\rho_{Cu0} = 1.667 \times 10^{-8}$ Ωm and $\alpha = 3.862 \times 10^{-3}$. The voltage is still defined using (4); however, $S$ now represents the cross-section including all wire layers.

### D. Electromagnetic-Thermal Coupling

To incorporate the thermal properties of the wire and investigate the effects of heating, a thermal model is coupled to the electromagnetic model using the following thermal transient equation:

$$\rho \cdot C \frac{dT}{dt} = \nabla \cdot (\kappa \nabla T) + Q \qquad (5)$$

where $Q$ is the heat source calculated in each layer of the wire from the product of the local electric field and current density, i.e., $Q = E_z \cdot J_z$.

For the HTS layer, the temperature-dependent thermal conductivity and specific heat presented in [38] are assumed and $\rho_{HTS} = 5900$ kg/m$^3$. A linear $J_c(T)$ is assumed such that $J_c(T) = J_{c0}(92 - T)/15$. For the substrate, the temperature-dependent thermal conductivity and specific heat presented in [37] are assumed and $\rho_{sub} = 8910$ kg/m$^3$. For the stabilizer layers, the temperature-dependent thermal conductivity presented in [39] and specific heat presented in [40] for Cu (RRR = 100) are assumed, and $\rho_{Cu} = 8940$ kg/m$^3$.

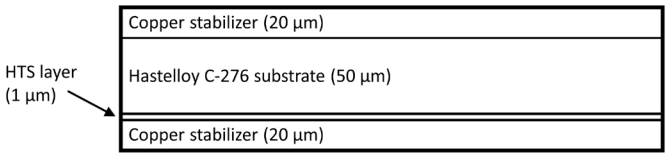


Fig. 3. Cross-sectional view of the modelled full wire architecture, including a 50 µm Hastelloy C-276 substrate and top and bottom 20 µm copper stabilizer layers, ignoring any copper surrounding the sides of the wire.

The HTS wire is assumed to be in a liquid nitrogen bath at 77 K. To simulate the thermal exchange between the wire and the bath, a convective heat flux boundary condition is applied to the outer boundaries of the wire, as described in [41-45]. The temperature-dependent heat transfer coefficent given in [41] is assumed, over the range $\Delta T = 0 - 30$ K, which takes into account heat transfer by free convection, nucleate boiling, transition boiling and film boiling regimes.

## III. Results

In the following, we consider three different models: the "HTS only" model includes only the HTS layer, neglecting the other layers of the wire architecture and the influence of the heat generated; the "Full wire" model includes all layers of the HTS wire, but neglects the heat generated; and the "Full wire, heat" model includes all layers of the HTS wire and includes the influence of the heat generated.

Fig. 4 shows the open-circuit DC output voltage of the HTS dynamo for the three models. The "HTS only" and "Full wire" models are calculated after 10 cycles of rotation. For the "Full

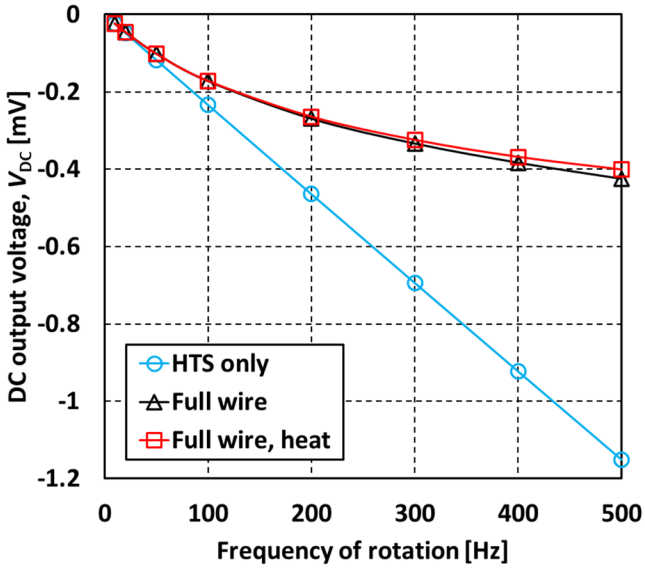


Fig. 4. Open-circuit DC output voltage of the HTS dynamo, as given by equation (4), for the three models. For the "HTS only" and "Full wire" models, these values are calculated after 10 cycles of rotation; for the "Full wire, heat" model, the number of cycles varies with frequency, ranging from 10 cycles up to 50 cycles to ensure thermal equilibrium is reached (see Fig. 5) and the DC output voltage is stable.

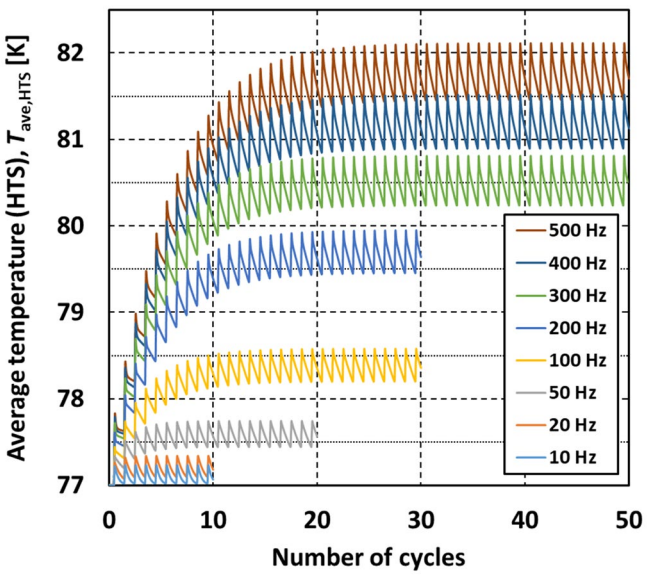


Fig. 5. Average temperature of the HTS layer for the "full wire" model with heat. The total number of cycles varies with frequency to ensure thermal equilibrium is reached and the DC output voltage (see Fig. 4) is stable.

wire, heat" model, the number of cycles varies with frequency, ranging from 10 cycles up to 50 cycles to ensure thermal equilibrium is reached and the DC output voltage is stable. The average temperature of the HTS layer in the "Full wire, heat" model is shown in Fig. 5. Additional data related to the instantaneous (time-dependent) output voltage, given by equation (2) and used to calculate the values shown in Fig. 4, can be found via the link in the Acknowledgment.

Up to around 50 Hz, all of the models produce a similar DC output voltage that increases linearly with increasing frequency. Above 50 Hz, the "HTS only" model continues to exhibit a linear increase in DC output voltage with increasing frequency, as expected from Faraday's law. However, for the "Full wire" and "Full wire, heat" models, the rate at which the

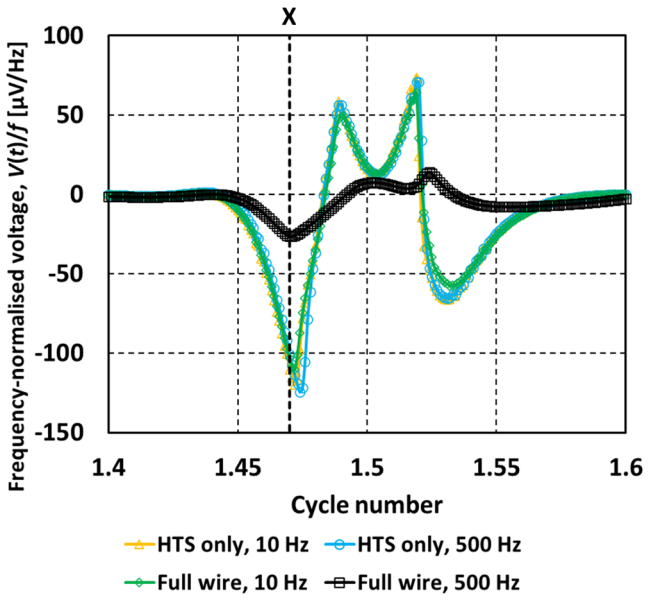


Fig. 6. Frequency-normalised instantaneous output voltage of the HTS dynamo for frequencies of rotation of 10 and 500 Hz for the "HTS only" and "full wire" models during the 2nd cycle of PM rotation.

DC output voltage increases reduces with increasing frequency, which becomes more noticeable above around 50 Hz, similar to that observed in experiments [16-19]. In addition, there is little difference observed with and without heating.

To further emphasise this deviation from linear behaviour as the frequency increases, Fig. 6 shows the frequency-normalised instantaneous output voltage of the HTS dynamo at 10 and 500 Hz for the "HTS only" and "Full wire" models during the 2nd cycle of PM rotation. For a voltage that increases linearly with frequency, one will expect that these curves will overlap. There is a noticeable difference for the full wire architecture model for 500 Hz: the voltage is significantly different in both magnitude and shape in comparison to the other three models.

These results, therefore, suggest that the dominant cause of the frequency-dependent behaviour of the open-circuit voltage of the HTS dynamo in this case is not heating, but some other mechanism related to the wire architecture. The various layers of a coated-conductor wire have indeed been shown to impact its electromagnetic behaviour, especially at high frequencies [46-49]. We now explore this point by interrogating the results from the developed models.

In the following, we consider the variation along the width of the HTS wire of the average (averaged along the thickness of each layer) electric field, $E_z$, and normalised current density, $J_z/J_{c0}$, as the PM approaches at $t$ = 1.47 cycles. This corresponds roughly to the first voltage peak in Fig. 6 (indicated by '**X**') and to an angle $\theta_M = 0.44\pi = 79.2°$ in Fig. 1.

Fig. 7 shows the results for the "HTS only" model for 10 and 500 Hz. In the region of the wire closest to the PM ($x$ = +6 mm), an overcritical current is induced to flow down this side

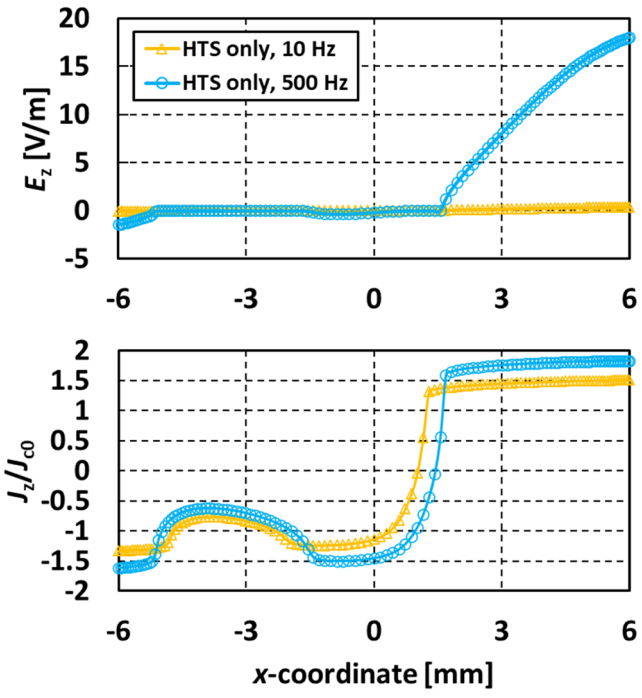


Fig. 7. "HTS only" model at 10 and 500 Hz: Average electric field, $E_z$ (top), and normalised current density, $J_z/J_{c0}$ (bottom), as the PM approaches the HTS wire ($t$ = 1.47 cycles).

of the wire by the local magnetic field from the rotating PM [7]. In the open-circuit configuration, an equal but opposite current returns on the other side of the wire ($x$ = –6 mm), but at a reduced critical current density [7]. It is also shown that the higher the frequency of rotation, the larger (or more overcritical) these eddy currents are: for $f$ = 10 Hz, $J_z/J_{c0} \approx 1.5$ at the edge of the wire, and for $f$ = 500 Hz, $J_z/J_{c0} \approx 1.83$.

Using equation (1), the expected electric field for such overcritical currents can be examined simply: for $J/J_c = 1.5$ and $n = 20$, $E = 3.325 \times 10^3 E_0 = 0.3325$ V/m; for $J/J_c = 1.83$ and the same $n$, $E = 177.4 \times 10^3 E_0 = 17.74$ V/m. These calculations agree well with the numerical results shown in Fig. 7. Assuming, for simplicity, that this electric field exists across the entire HTS layer, and is in parallel with a copper sheet of the same width (12 mm), thickness 20 μm and $\rho_{Cu}$(77 K) = $2.75 \times 10^{-9}$ Ωm, then $J_{Cu} = 1.21 \times 10^8$ A/m$^2$ for $J/J_c = 1.5$ and $J_{Cu} = 6.45 \times 10^9$ A/m$^2$ for $J/J_c = 1.83$. This latter value is an extremely high current density for copper. By way of illustration, a unidirectional transport current flowing through the entire copper sheet at the same current density would correspond to $I_{Cu}$ = 1548 A >> $I_{c0}$ (cf. $I_{HTS} = 1.83 \times 283 = 517.9$ A). Hence, as the frequency of rotation increases, $J/J_c$ subsequently increases, and more current will divert into the copper stabilizer layers. From Fig. 4, this effect in this case becomes significant for $f$ > 50 Hz.

Now, we consider the "Full wire" model. Figs. 8 and 9 show the average electric field, $E_z$, and normalised current density, $J_z/J_{c0}$, as the PM approaches the HTS wire (again, $t$ = 1.47 cycles) for 10 and 500 Hz, respectively. The behaviour of the wire in Fig. 8 (10 Hz) is much the same as the "HTS only, no heat" model, with essentially the same open-circuit voltage (see Fig. 6) and electric field and current density (see Fig. 7). However, at 500 Hz, as shown in Fig. 9, there are a number of key differences:

1) A substantial current now flows in the top and bottom copper stabilizer layers. At the edge closest to the PM ($x$ = +6 mm), $J \approx 0.2 J_{c0}$ flows in the copper layers.

2) $J_z/J_{c0}$ in the HTS layer in the region close to the PM is slightly reduced, but also flows over a reduced width of wire (approx. 3 mm, instead of 4 mm in the "HTS only" model). This suggests that the HTS layer becomes increasingly shielded by the stablizer layers as the frequency increases;

3) $J_z/J_{c0}$ for the return current is higher when including the full wire architecture and flows over a wider region, indicating an increase in return current; and

4) The electric field is substantially reduced in the region close to the PM (related to point 2) above) and increases for the return path (related to point 3) above). The voltage as defined by equation (2) is therefore reduced significantly.

Thus, all these factors combine to reduce the output voltage of the HTS dynamo in the full wire model, resulting in a frequency-dependence that is in contrast to the expected linear behavior. In this particular configuration (a single PM rotating past a single HTS wire with top and bottom copper stablizer layers in a liquid nitrogen bath), the heat generated appears to have little effect. It should be noted that the generated heat is likely to have more impact for other HTS dynamo configurations (e.g., a multiple magnet rotor) and other HTS wire architectures (e.g., stablizer-free wires), which will be of great interest for future studies. Simple modifications to this fast and efficient modelling framework allow the exploration of the influence of the HTS dynamo design on its DC output voltage and other parameters of interest.

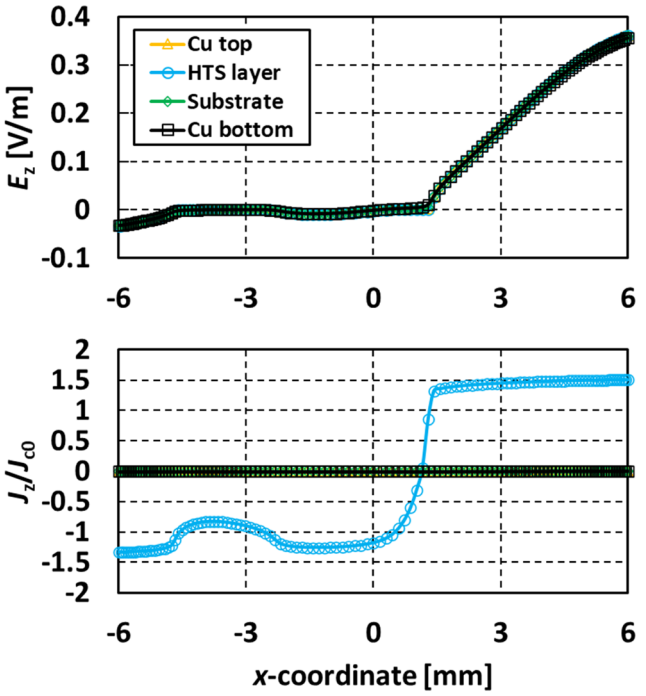


Fig. 8. "Full wire" model at 10 Hz: Average electric field, $E_z$ (top), and normalised current density, $J_z/J_{c0}$ (bottom), as the PM approaches the HTS wire ($t$ = 1.47 cycles).

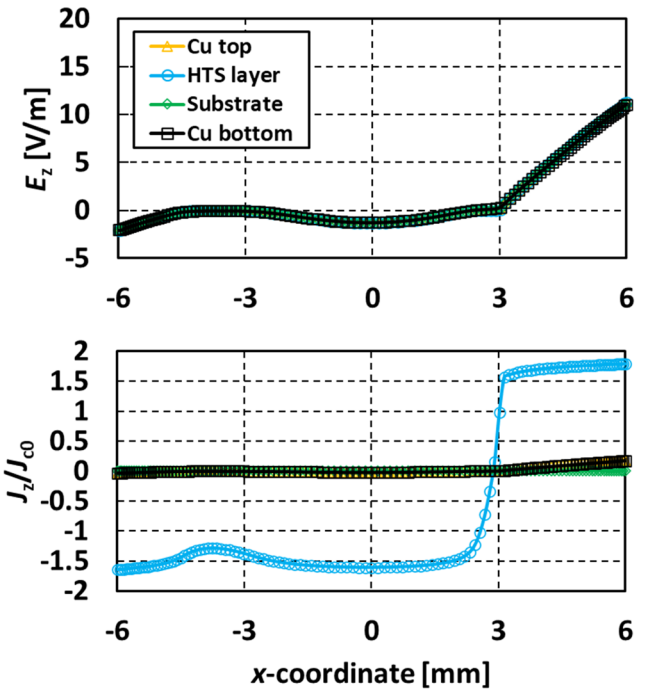


Fig. 9. "Full wire" model at 500 Hz: Average electric field, $E_z$ (top), and normalised current density, $J_z/J_{c0}$ (bottom), as the PM approaches the HTS wire ($t$ = 1.47 cycles).

## IV. Conclusion

The HTS dynamo enables the injection of large DC currents into a superconducting circuit, without the requirement for current leads connected from the cryogenic environment to the room temperature. This has significant potential to be used to energise HTS coils in NMR/MRI magnets and superconducting rotating machines. In this work, a segregated ***H***-formulation finite-element model, which provides an efficient way of modelling the relative movement between the rotating room-temperature permanent and the static HTS wire, is extended to include the full HTS wire architecture and coupled with a thermal model. This modelling framework is used to explain the experimentally-observed frequency-dependence of such dynamos/flux pumps, where the rate at which the open-circuit voltage increases reduces with increasing frequency, in contrast to the expected linear behavior. It is shown that the dominant cause of this behaviour, in the case investigated here based on the HTS dynamo benchmark problem, is the interaction between and current flow in the different layers of the HTS wire. Heat generated – the common explanation given to date – is shown to have much less influence on the frequency behaviour in comparison.

## Acknowledgment

Data related to this publication are available at the University of Cambridge data repository [https://doi.org/10.17863/CAM.58900].

## References

[1] C. Hoffmann, D. Pooke, and A. D. Caplin, "Flux Pump for HTS Magnets," *IEEE Trans. Appl. Supercond.*, vol. 21, no. 3, pp. 1628-31, Jun. 2011.

[2] J. Volger and P. S. Admiraal, "A dynamo for generating a persistent current in a superconducting circuit," *Phys. Lett.*, vol. 2, no. 5, pp. 257-9, Oct. 1962.

[3] H. V. Beelen *et al.*, "Flux pumps and superconducting solenoids," *Physica*, vol. 31, no. 4, pp. 413-43, Apr. 1965.

[4] C. W. Bumby *et al.*, "Development of a brushless HTS exciter for a 10 kW HTS synchronous generator," *Supercond. Sci. Technol.*, vol. 29, no. 2, Art. no. 024008, Feb. 2016.

[5] Z. Bai *et al.*, "A novel high temperature superconducting magnetic flux pump for MRI magnets," *Cryogenics*, vol. 50, no. 10, pp. 688-92, Oct. 2010.

[6] M. D. Ainslie *et al.*, "A new benchmark problem for electromagnetic modelling of superconductors: the high-$T_c$ superconducting dynamo," *Supercond. Sci. Technol.*, vol. 33, no. 10, Art. no. 105009, Oct. 2020.

[7] R. C. Mataira, M. D. Ainslie, R. A. Badcock, and C. W. Bumby, "Origin of the DC output voltage from a high-$T_c$ superconducting dynamo," *Appl. Phys. Lett.*, vol. 114, no. 16, Art no. 162601, Apr. 2019.

[8] R. Mataira *et al.*, "Mechanism of the High-$T_c$ Superconducting Dynamo: Models and Experiment," *Phys. Rev. Appl.*, vol. 14, no. 2, Art. no. 024012, Aug. 2020.

[9] J. Geng *et al.*, "Voltage-ampere characteristics of YBCO coated conductor under inhomogeneous oscillating magnetic field," *Appl. Phys. Lett.*, vol. 108, no. 26, Art. no. 262601, Jun. 2016.

[10] J. Geng *et al.*, "Origin of dc voltage in type II superconducting flux pumps: field, field rate of change, and current density dependence of resistivity," *J. Phys. D*, vol. 49, no. 11, Art. no. 11LT01, Feb. 2016.

[11] C. W. Bumby *et al.*, "Anomalous open-circuit voltage from a high-$T_c$ superconducting dynamo," *Appl. Phys. Lett.*, vol. 108, no. 12, Art no. 122601, Mar. 2016.

[12] Z. Jiang *et al.*, "Dynamic resistance of a high-$T_c$ superconducting flux pump," *Appl. Phys. Lett.*, vol. 105, no. 11, Art. no. 112601, Sep. 2014.

[13] V. S. Vysotsky *et al.*, "The possibility of using high-$T_c$ superconducting films as elements of a rectifier," *Supercond. Sci. Technol.*, vol. 3, no. 5, pp. 259-262, May 1990.

[14] A. Ghabeli and E Pardo, "Modeling of airgap influence on DC voltage generation in a dynamo-type flux pump", *Supercond. Sci. Technol.*, vol. 33, no. 3, Art. no. 035008, Feb. 2020.

[15] R. Mataira, M. D. Ainslie, R. Badcock, and C. W. Bumby, "Modeling of Stator Versus Magnet Width Effects in High-$T_c$ Superconducting Dynamos," *IEEE Trans. Appl. Supercond.*, vol. 30, no. 4, Art. no. 5204406, Jun. 2020.

[16] A. E. Pantoja, Z. Jiang, R. A. Badcock, and C. W. Bumby, "Impact of Stator Wire Width on Output of a Dynamo-Type HTS Flux Pump," *IEEE Trans. Appl. Supercond.*, vol. 26, no. 8, Art. no. 4805208, Dec. 2016.

[17] C. W. Bumby *et al.*, "Frequency Dependent Behavior of a Dynamo-Type HTS Flux Pump," *IEEE Trans. Appl. Supercond.*, vol. 27, no. 4, Art. no. 5200705, Jun. 2017.

[18] A. E. Pantoja *et al.*, "Output During Continuous Frequency Ramping of a Dynamo-Type HTS Flux Pump," *IEEE Trans. Appl. Supercond.*, vol. 28, no. 3, Art. no. 5202205, Apr. 2018.

[19] J. G. Storey *et al.*, "Optimizing Rotor Speed and Geometry of an Externally Mounted HTS Dynamo," *IEEE Trans. Appl. Supercond.*, vol. 29, no. 5, Art. no. 5202705, Aug. 2019.

[20] L. Quéval *et al.*, "Superconducting magnetic bearings simulation using an H-formulation finite element model," *Supercond. Sci. Technol.*, vol. 31, no. 8, Art no. 084001, Aug. 2018.

[21] R. A. Badcock *et al.*, "Impact of Magnet Geometry on Output of a Dynamo-Type HTS Flux Pump," *IEEE Trans. Appl. Supercond.*, vol. 27, no. 4, Art. no. 5200905, Jun. 2017.

[22] K. Kajikawa *et al.*, "Numerical evaluation of AC losses in HTS wires with 2D FEM formulated by self magnetic field," *IEEE Trans. Appl. Supercond.*, vol. 13, no. 2, pp. 3630-3, Jul. 2003.

[23] R. Pecher *et al.*, "3D-modelling of bulk type-II superconductors using unconstrained H-formulation," *Proc. 6th EUCAS Conf.*, 14-18 Sept. 2003, Sorrento, Italy, pp 1-11.

[24] Z. Hong, A. M. Campbell, and T. A. Coombs, "Numerical solution of critical state in superconductivity by finite element software," *Supercond. Sci. Technol.*, vol. 19, no. 12, pp. 1246-52, Oct. 2006.

[25] R. Brambilla, F. Grilli, and L. Martini, "Development of an edge-element model for AC loss computation of high-temperature superconductors," *Supercond. Sci. Technol.*, vol. 20, no. 1, pp. 16-24, Nov. 2006.

[26] M. D. Ainslie, T. J. Flack, Z. Hong, and T. A. Coombs, "Comparison of first- and second-order 2D finite element models for calculating AC loss in high temperature superconductor coated conductors," *Int. J. Comput. Math. Electr. Electron. Eng.*, vol. 30, no. 2, pp. 762-74, Mar. 2011.

[27] M. D. Ainslie *et al.*, "Modeling and Electrical Measurement of Transport AC Loss in HTS-Based Superconducting Coils for Electric Machines," *IEEE Trans. Appl. Supercond.*, vol. 21, no. 3, pp. 3265-8, Jun. 2011.

[28] M. D. Ainslie, T. J. Flack, and A. M. Campbell, "Calculating transport AC losses in stacks of high temperature superconductor coated conductors with magnetic substrates using FEM," *Physica C*, vol. 472, no. 1, pp. 50-6, Jan. 2012.

[29] C. J. G. Plummer and J. E. Evetts, "Dependence of the shape of the resistive transition on composite inhomogeneity in multifilamentary wires," *IEEE Trans. Magn.*, vol. 23, no. 2, pp. 1179-82, Mar. 1987.

[30] J. Rhyner, "Magnetic properties and AC-losses of superconductors with power law current-voltage characteristics," *Physica C*, vol. 212, no. 3-4, pp. 292-300, Jul. 1993.

[31] E. H. Brandt, "Susceptibility of superconductor disks and rings with and without flux creep," *Phys. Rev. B*, vol. 55, no. 21, pp. 14513-26, Jun. 1997.

[32] F. Grilli *et al.*, "Computation of Losses in HTS Under the Action of Varying Magnetic Fields and Currents," *IEEE Trans. Appl. Supercond.*, vol. 24, no. 1, Art. no. 8200433, Feb. 2014.

[33] M. D. Ainslie and H. Fujishiro, "Modelling of bulk superconductor magnetization," *Supercond. Sci. Technol.*, vol. 28, no. 5, 2015, Art. ID 053002, Mar. 2015.

[34] W. Yang *et al.*, "A 3-D Strong-Coupled Electromagnetic-Thermal Model for HTS Bulk and Its Uses to Study the Dynamic Characteristics of a Linear HTS Maglev Bearing," *IEEE Trans. Appl. Supercond.*, vol. 30, no. 6, Art. no. 3602814, Sep. 2020.

[35] K. Liu *et al.*, "Experiment and simulation of superconducting magnetic levitation with REBCO coated conductor stacks," *Supercond. Sci. Technol.*, vol. 31, no. 1, Art. no. 015013, Jan. 2018.
[36] SuperPower Inc. [http://www.superpower-inc.com/]
[37] J. Lu, E. S. Choi, and H. D. Zhou, "Physical properties of Hastelloy® C-276™ at cryogenic temperatures," *J. Appl. Phys.*, vol. 103, no. 6, Art. no. 064908, Mar. 2008.
[38] M. Zhang, K. Matsuda, and T. A. Coombs, "New application of temperature-dependent modelling of high temperature superconductors: Quench propagation and pulse magnetization," *J. Appl. Phys.*, vol. 112, no. 4, Art. no. 043912, Aug. 2012.
[39] National Institute of Standards and Technology (NIST) Cryogenics Material Properties database [https://trc.nist.gov/cryogenics/materials/materialproperties.htm]
[40] X. Wang, U. P. Trociewitz, and J. Schwartz, "Near-adiabatic quench experiments on short $YBa_2Cu_3O_{7-\delta}$ coated conductors," *J. Appl. Phys.*, vol. 101, no. 5, Art. no. 053904, Mar. 2007.
[41] T. Rettelbach and G. J. Schmitz, "3D simulation of temperature, electric field and current density evolution in superconducting components," *Supercond. Sci. Technol.*, vol. 16, no. 5, pp. 645-653, May 2003.
[42] J. Duron *et al.*, "Finite-element modelling of YBCO fault current limiter with temperature dependent parameters," *Supercond. Sci. Technol.*, vol. 20, no. 4, pp. 338-344, Apr. 2007.
[43] F. Roy, B. Dutoit, F. Grilli, and F. Sirois, "Magneto-Thermal Modeling of Second-Generation HTS for Resistive Fault Current Limiter Design Purposes," *IEEE Trans. Appl. Supercond.*, vol. 18, no. 1, pp. 29-35, Mar. 2008.
[44] W. T. B. de Sousa, A. Polasek, C. F. T. Matt, and R. de Andrade, Jr., "Recovery of Superconducting State in an R-SCFCL MCP-BSCCO-2212 Assembly," *IEEE Trans. Appl. Supercond.*, vol. 23, no. 1, Art. no. 5601407, Feb. 2013.
[45] S. Liang *et al.*, "Study on Quenching Characteristics and Resistance Equivalent Estimation Method of Second-Generation High Temperature Superconducting Tape under Different Overcurrent," *Materials*, vol. 12, no. 15, Art. no. 2374, Aug. 2019.
[46] G. Liu *et al.*, "Experimental and numerical study of frequency-dependent transport loss in $YBa_2Cu_3O_{7-\delta}$ coated conductors with ferromagnetic substrate and copper stablizer," *J. Appl. Phys.*, vol. 121, no. 24, Art. no. 243902, Jun. 2017.
[47] P.-B. Zhou, G.-T. Ma, and L. Quéval, "Transition frequency of transport AC losses in high temperature superconducting coated conductors," *J. Appl. Phys.*, vol. 126, Art. no. 063901, Jul. 2019.
[48] P.-B. Zhou *et al.*, "Frequency-dependent transport AC losses of coated superconductors up to tens of kilohertz," *IEEE Trans. Appl. Supercond.*, vol. 29, no. 5, Art. no. 8201705, Aug. 2019.
[49] H. Zhang *et al.*, "Modelling of electromagnetic loss in HTS coated conductors over a wide frequency band," *Supercond. Sci. Technol.*, vol. 33, no. 2, Art. no. 025004, Feb. 2020.